Structural Stability of Super Duplex Stainless Weld Metals and Its Dependence on Tungsten and Copper

J.-O. NILSSON, T. HUHTALA, P. JONSSON, L. KARLSSON, and A. WILSON

Three different superduplex stainless weld metals have been produced using manual metal arc welding under identical welding conditions. The concentration of the alloying elements tungsten and copper corresponded to the concentrations in commercial superduplex stainless steels (SDSS). Aging experiments in the temperature range 700 °C to 1110 °C showed that the formation of intermetallic phase was enhanced in tungsten-rich weld metal and also dissolved at higher temperatures compared with tungsten-poor and tungsten-free weld metals. It could be inferred from time-temperature-transformation (TTT) and continuous-cooling-transformation (CCT) diagrams produced in the present investigation that the critical cooling rate to avoid 1 wt pct of intermetallic phase was 2 times faster for tungsten-rich weld metal. Microanalysis in combination with thermodynamic calculations showed that tungsten was accommodated in χ phase, thereby decreasing the free energy. Experimental evidence supports the view that the formation of intermetallic phase is enhanced in tungsten-rich weld metal, owing to easier nucleation of nonequilibrium χ phase compared with σ phase. The formation of secondary austenite (γ_2) during welding was modeled using the thermodynamic computer program Thermo-Calc. Satisfactory agreement between theory and practice was obtained. Thermo-Calc was capable of predicting observed lower concentrations of chromium and nitrogen in γ_2 compared with primary austenite. The volume fraction of γ_2 was found to be significantly higher in tungsten-rich and tungsten + copper containing weld metal. The results could be explained by a higher driving force for precipitation of γ_2 in these.

I. INTRODUCTION

DUPLEX stainless steels (DSS) constitute a group of very attractive steels possessing a favorable combination of mechanical strength and corrosion resistance in chloride ion containing environments. Superduplex stainless steels (SDSS) are characterized by an unusually high resistance to pitting corrosion and are commonly defined as the subset of DSS that shows a pitting resistance equivalent (PRE_N = wt pct Cr + 3.3 × wt pct Mo + 16 × wt pct N) above 40. The resistance to pitting corrosion in the base material can be optimized by selecting a diffusion annealing temperature which is such that the concentration of alloying elements corresponds to equal pitting resistance in ferrite and austenite. However, the situation in the weld metal is more complex than in the base metal, since the advantages of diffusion annealing cannot be used. The balance of alloying elements can be disturbed, either by the formation of intermetallic precipitates and Cr_2N or by excessive precipitation of so-called secondary austenite (γ_2). Redistribution of alloying elements, as a result of such transformations, may lead to local reductions in pitting resistance and associated corrosion attack, either in regions that are depleted with respect to crucial alloying elements or in the precipitates themselves.

In theory, pitting corrosion resistance in DSS could be further improved by additions of chromium, molybdenum, and nitrogen. However, since these elements also promote the formation of intermetallic precipitates such as σ phase, χ phase, and R phase and nitrides,[1] there are practical limits regarding the amount of alloying additions. It has recently been suggested that tungsten in superduplex stainless steel base metal improves the resistance to pitting corrosion but, unlike molybdenum, hinders the formation of intermetallic phase.[2] This contradicts findings by Charles,[3] who reports faster precipitation kinetics and a higher dissolution temperature of intermetallic phase as a result of tungsten additions and thereby points out similarities rather than differences between tungsten and molybdenum.

The kinetics of austenite formation is also of importance for the following reason. The DSS are almost entirely ferritic at temperatures just below solidus. However, on cooling, transformation of ferrite to austenite will occur.[1,4] The austenite formed in this manner at relatively high temperatures is usually termed primary austenite. Additional transformation of ferrite to γ_2 may occur after the duplex structure has been established, *e.g.*, during a subsequent isothermal heat treatment or during reheating in association with welding. There appear to be essentially two types of γ_2, one occurring at the austenite/ferrite phase boundaries[5] and one occurring in the interior of ferrite grains.[6] Which of the two is predominant is determined by the existence of suitable nuclei. The type of γ_2 found in weld metal is essentially of the intragranular type,[6] while γ_2 at the phase boundaries is characteristic of isothermal treatment of the base metal.[5] A likely explanation is that nucleation of γ_2 in the interior of grains is facilitated in the weld metal compared with the base metal by the quenched-in stresses and vacancy clusters in combination with the larger number of inclusions that are typical of welded structures.[7]

J.-O. NILSSON, Manager, Physical Metallurgy, and A. WILSON, Research Metallurgist, Tube Laboratory, are with the R&D Center, AB Sandvik Steel, S-811 81, Sandviken, Sweden. T. HUHTALA, Research Metallurgist, and L. KARLSSON, Senior Research Metallurgist, are with Central Laboratories, Esab AB, S-402 77, Göteborg, Sweden. P. JONSSON, Graduate Student, Department of Engineering Materials, is with the Luleå University of Technology, S-951 63, Luleå, Sweden.

Manuscript submitted April 11, 1995.

Table I. Chemical Composition of Weld Metals Obtained from OES and Nominal Composition of SAF 2507 Plate

	Si	Mn	Cr	Ni	Mo	W	Cu	C	N
SAF 2507	≤0.8	≤1.2	25.0	6.9	4.0	—	≤0.5	≤0.03	0.27
SDH*	0.71	0.70	25.66	9.24	3.80	<0.003	0.09	0.034	0.26
WCuH	0.38	0.86	25.17	9.21	3.61	0.89	0.63	0.035	0.23
WH	0.66	1.31	25.49	9.50	3.12	2.14	0.10	0.043	0.25
SDN**	0.75	0.72	25.59	9.26	3.79	<0.003	0.09	0.034	0.25
WCuN	0.38	0.93	25.47	9.20	3.60	0.92	0.62	0.038	0.23
WN	0.69	1.34	25.67	9.60	3.09	2.34	0.09	0.046	0.24

*H denotes high heat input (1.4 kJ/mm)
**N denotes normal or low heat input (0.8 kJ/mm).

Adverse effects of intermetallic precipitates[8,9] and γ_2[10] on corrosion resistance have been observed and are well known. The aim of the present work was to establish the precipitation kinetics of these phases in relation to chemical composition. This work is included in a larger project in which also the corrosion and mechanical properties were assessed.[11] Particular attention was paid to the role of elements such as copper and tungsten that are used in certain SDSS to enhance the corrosion resistance. Furthermore, there was a desire to quantify, both experimentally and theoretically, the concentration in welding-induced intragranular secondary austenite of chromium, molybdenum, and nitrogen, all of which are crucial elements in preventing pitting corrosion. Since there is no single technique that is suitable for analyzing all these elements, a combination of energy dispersive X-ray (EDX) analyses in the analytical transmission electron microscope, wavelength dispersive X-ray (WDX) analysis in the electron microprobe, and thermodynamic computer calculations was employed.

II. EXPERIMENTAL

A. *Experimental Material*

Superduplex stainless steel plates of dimensions 300 × 200 × 20 mm were welded together in a horizontal position using three different filler metals under identical conditions employing multipass welding of a V-joint according to ISO 2560. Manual metal arc welding was used at two different heat inputs, *viz.* 0.8 kJ/mm (denoted by N) and 1.4 kJ/mm (denoted by H). The number of beads was 14 at 1.4 kJ/mm and 24 at 0.8 kJ/mm and air cooling between the runs guaranteed an interpass temperature not exceeding 100 °C.

The chemical composition of the superduplex stainless steel plates was in accordance with the specification of Sandvik SAF 2507, the nominal composition of which is given in Table I. Filler metals of three types with the basic composition 25 pct* chromium, 9 pct nickel, 3 to 4 pct molybdenum, and 0.25 pct nitrogen were used. Covered electrodes of a type equivalent to Sandvik 25.10.4.LR and Esab OK 68.53 were chosen as references (termed SD for simplicity in the following). Of the other two filler metals, one was alloyed with tungsten and copper (denoted by WCu) and the other with tungsten only (denoted by W). In the case of W-weld metal, tungsten was added *via* the electrode coating, while in WCu-weld metal, tungsten and copper were added through commercially available core wire. The welding resulted in six weld metals in total, the compositions of which are given in Table I. The analysis was performed using optical emission spectroscopy (OES) from a 6-mm-diameter spot in the center of the weld metal in its as-welded condition. All specimens used in the following investigations were also taken from the central parts of the weld metal.

*When not specified, it is implicitly assumed in the following that all concentrations are in weight percent.

Intermetallic phases were investigated only in samples taken from weld metal obtained at the lowest heat input, 0.8 kJ/mm, with the approximate dimensions 12 × 11 × 2 mm. Isothermal heat treatment was carried out by immersion in salt bath. This guaranteed efficient heat transfer with associated rapid heating. Isothermal aging was performed in the temperature range 700 °C to 1050 °C from 30 seconds up to 121.5 minutes. Each heat treatment was followed by water quenching. An air furnace was used for heat treatments ranging from 1050 °C to 1110 °C to assess the exact dissolution temperature for intermetallic phase.

B. *Estimation of CCT Diagrams*

Time-temperature-transformation (TTT) diagrams were determined from point counting as described subsequently. These formed the basis for calculating continuous-cooling-transformation (CCT) diagrams according to a procedure described in detail by Josefsson *et al.*,[12] whereby the cooling curve was approximated by a series of small isothermal steps. It was assumed in these calculations that the evolution of intermetallic phase could be described by an Avrami equation of the type

$$\frac{V}{V_m(T)} = 1 - e^{-b(T)t^{n(T)}}$$

where V is the volume fraction of intermetallic phase, V_m is the corresponding equilibrium fraction at temperature T, $b(T)$ and $n(T)$ are temperature-dependent quantities, and t is time. The values $b(T)$ and $n(T)$ are experimentally determined and optimized from the preceding Avrami equation using isothermal data. It was also assumed, based on aging experiments performed at 1000 °C (*cf.* Table V), that the equilibrium volume fraction of intermetallic phase was 0.25 for SD- and WCu-weld metal and 0.35 for W-weld metal. A quench dilatometer of the type Dilatronic III was used to simulate cooling operations, whereby the validity of the calculated CCT diagram could be checked. Dilatometer specimens of the size 11 × 2.5 × 2 mm from as-welded weld metal were heated at a rate of 10 °C/s to 1100 °C for SD and WCu material and 1150 °C for W material. After

a hold time of 5 minutes in vacuum, controlled cooling to ambient temperature was accomplished by flushing with helium gas. Five different cooling rates ranging between 45 °C/min and 720 °C/min were used.

C. *Microanalysis*

Light optical microscopy (LOM) was made in a Reichert Univar instrument, which was also used to estimate the volume fraction of intermetallic phase and γ_2 by point counting according to ISO 9042. A grid with 20 points was used in these measurements. As many as 50 fields were used, resulting in a total number of 1000 points. The statistical uncertainty was estimated using the procedure described in ISO 9042. Contrast from intermetallic phase was produced using a two-step electrolytic etching technique involving dilute nitric acid to make phase boundaries visible followed by saturated potassium hydroxide to enhance the contrast from the precipitates. It was found that etching using type Beraha etchant[13] produced as-welded microstructures with γ_2 in high contrast. The Beraha etchant involves 2.2 g $(NH_4)HF_2$, 0.2 g $K_2S_2O_5$, 18 mL HCl, and 100 mL distilled H_2O. Etching for a time in the range 10 to 20 seconds colors ferrite blue while austenite remains virtually uncolored.

An independent way of measuring the volume fraction of austenite and ferrite was provided by the magnetic balance, which is an instrument composed of an electromagnet, which generates an inhomogeneous electromagnetic field of a magnitude of 987 kA/m, and a balance, which measures the magnetic force.[14] The specimen weight is typically 1 g for DSS having a percentage of ferrite ranging between 10 and 90 pct. This force can be calibrated against the volume fraction of magnetic phase estimated *via* point counting in an LOM.

Scanning electron microscopy was performed in a JEOL* JSEM 840 provided with a LINK AN10000 unit for EDX analysis. Thin foil specimens for analytical transmission electron microscopy (ATEM) were prepared by electrochemical polishing in a solution of 15 pct perchloric acid in methanol. The foils were examined in an ATEM of type JEOL 2000FX provided with an EDX detector of the same type as that described earlier. Quantitative EDX analyses of thin foils in ATEM were performed using the ratio thin section program provided by the WDX analysis was performed in an electron probe microanalyzer (EPMA) of type Cameca Camebax SX 50. The WDX analysis in the EPMA is a valuable complement to EDX, since higher electron beam currents allow measurements of concentrations with a higher accuracy. The accuracy was in the present case typically 0.1 wt pct for the metallic elements and 0.05 wt pct for nitrogen. Moreover, in contrast to EDX, light elements such as nitrogen can be analyzed both qualitatively and quantitatively. A limitation in the EPMA is the spatial resolution, which is of the order 1 μm, a figure that should be compared with 20 nm that is a typical value of the lateral resolution of EDX analysis in the ATEM. Since secondary austenite grains were only a few micrometers in diameter, there was an apparent risk of contribution to the X-ray signal from the surrounding ferrite when γ_2 was analyzed by WDX. To improve the spatial resolution in the EPMA, analyses were performed using the lowest possible accelerating voltage, *viz.* 10 kV. However, occasionally, chromium concentrations approaching that of ferrite were measured in γ_2. Such experimental values and their corresponding nitrogen concentrations were omitted. This criterion of validity therefore was considered to give relevant concentrations of nitrogen in γ_2.

*JEOL is a trademark of Japan Electron Optics Ltd., Tokyo.

D. *Thermodynamic Equilibrium Calculations*

Thermo-Calc, a computer program for phase diagram calculations developed by Sundman *et al.*,[15] was used in simulating the process of precipitation of secondary austenite in superduplex weld metals. The program calculates the minimum Gibbs energy for the most stable set of phases considered using functions fitted to various experimental thermodynamic data such as activities, equilibrium tie-lines, and solubilities. This approach provided a powerful means of analyzing compositional data obtained from the different types of analytic instruments used in the present work. The formation of γ_2 during multipass welding is envisaged as a decomposition of ferrite caused by reheating of underlying weld beads resulting in γ_2 precipitation essentially in the grain interior. However, the model used to simulate the phase transitions occurring during welding only relates to the chemical composition of the phases involved and is therefore independent of assumptions of nucleation site. It was assumed that primary austenite and ferrite formed at 1300 °C and that a short time at 1300 °C was sufficient to establish equilibrium. Two approaches were used to model the formation of secondary austenite. In both cases, it was assumed that γ_2 formed at 800 °C. In case 1, it is assumed that γ_2 attains true equilibrium with primary austenite and ferrite. This implies that primary austenite and γ_2 in case 1 will have identical compositions, the only difference being the origin of formation. Case 2 considers the situation in which γ_2 is in equilibrium only with the surrounding ferrite grain in which it is formed, while the composition of the primary austenite is left unchanged. Case 2 therefore requires that no exchange of alloy elements occurs between primary austenite and ferrite. It is believed that the real situation falls in between these extremes.

III. RESULTS

A. *Microstructure*

1. *Unaged weld metal*

Weld metal in as-welded condition was in all cases found to be virtually devoid of intermetallic precipitates and nitrides. However, small intragranular precipitates of γ_2 were clearly visible in ferrite. It was qualitatively observed that the volume fraction of γ_2 was higher in WCu- and in W-weld metal compared with SD-weld metal irrespective of heat input. Results from point counting in LOM are presented in Table II. It should be mentioned that the percentage of ferrite was defined as the complement of all austenite. For comparison, volume percentages of ferrite obtained using magnetic balance are quoted in parentheses. It is clear from Table II that the magnetic balance gives systematically higher values than point counting.

It can be concluded from Table II that there is no sig-

Table II. Volume Percentage of Phases in As-Welded Material Obtained by Point Counting

	Ferrite	Austenite	Secondary Austenite
SDH	30.5(37.9)*	68.6 ± 2.7	0.9 ± 0.9
WCuH	24.3(35.0)	70.6 ± 3.4	5.1 ± 1.6
WH	29.8(36.1)	66.6 ± 2.9	3.6 ± 1.3
SDN	29.4(38.6)	69.7 ± 2.6	0.9 ± 0.8
WCuN	25.9(30.9)	69.2 ± 2.6	4.9 ± 1.8
WN	27.3(34.4)	68.7 ± 3.7	4.0 ± 1.8

*Numbers in parentheses refer to results obtained using magnetic balance.

nificant effect of heat input in the range 0.8 to 1.4 kJ/mm on the volume fraction of γ_2. The SD-weld metal has a volume fraction of γ_2 that is about 1 pct, which is barely measurable using point counting. This number is significantly less than 4 to 5 pct, which is a representative number for W- and WCu-weld metal. However, no mutual ranking of W- and WCu-weld metal could be made, owing to statistical uncertainties.

Light optical microscopy showed that γ_2 was inhomogeneously distributed both in the weld metal and within the individual weld beads. Austenite γ_2 was often found in upper parts of underlying weld beads, while areas in weld beads immediately above were often free of γ_2. In W- and WCu-weld metal, γ_2 could sometimes be observed in the outermost surface in top beads, while γ_2 in SD-weld metal was confined to the interior.

Representative micrographs from scanning electron microscopy (SEM) of weld metal in the as-welded condition are shown in Figures 1(a) through (c) in which γ_2 appears in bright contrast. Figure 2 shows a ferrite grain at higher magnification in WH-weld metal in which a large number of γ_2 grains has formed. As shown in Figure 2, a large number of γ_2 grains have sharp edges. Some of these also have a mirror plane in the center, as pointed out in Figure 2 with an arrow. This type of γ_2 was found to be more common at high heat inputs. Investigations in ATEM showed that the mirror plane in the center of such γ_2 grains was a twin boundary, the adjacent crystals being mutual twins (Figure 3). It should be pointed out, however, that globular γ_2 was present in all material conditions, an example of which is given in Figure 4. In some cases, the density of γ_2 was so high that a so-called basket weave structure was formed. This structure was observed particularly in W- and WCu-weld metals in which the volume fraction of γ_2 was highest. An example of a basket weave structure observed in WN weld metal is shown in Figure 5.

2. *Aged weld metal*

The intermetallic phase observed by LOM was subjected to electron diffraction analysis in ATEM. Careful analyses showed that the intermetallic precipitates were of three kinds, *viz.* σ phase, χ phase, and R phase. A summary of the results obtained in the three weld metals is given in Table III. At 700 °C/40.5 min, χ phase and R phase were observed in all weld metals while no evidence of σ phase was found. The predominant phase in SD- and W-weld metal was R phase, while χ phase predominated in WCu-weld metal. The R phase exclusively showed the well-de-

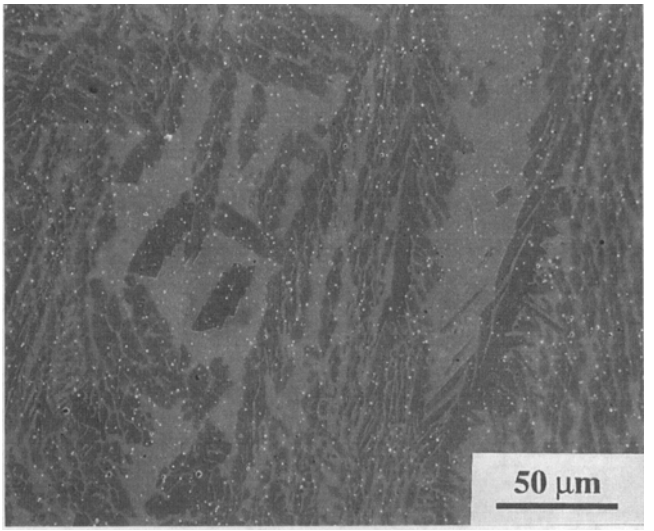

(*a*)

(*b*)

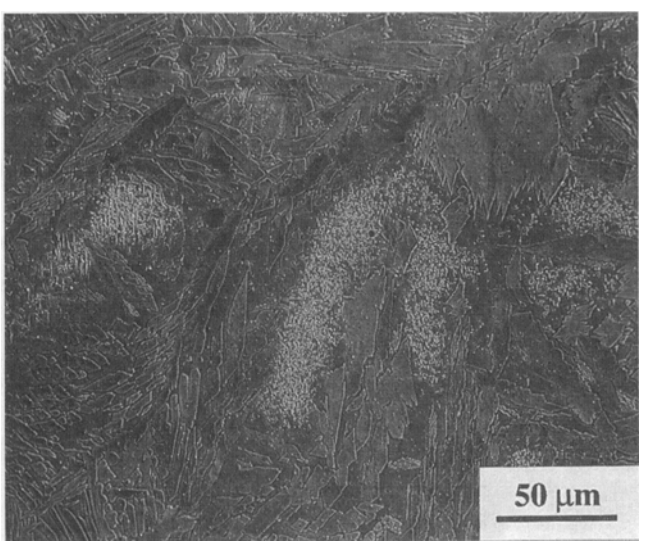

(*c*)

Fig. 1—(*a*) Microstructure in SDH-weld metal observed in SEM. Ferrite regions are almost free of γ_2. (*b*) Microstructure in WCuH-weld metal observed in SEM. Regions of ferrite that are rich in γ_2 appear in bright contrast. (*c*) Microstructure in WH-weld metal observed in SEM. Regions of ferrite that are rich in γ_2 appear in bright contrast.

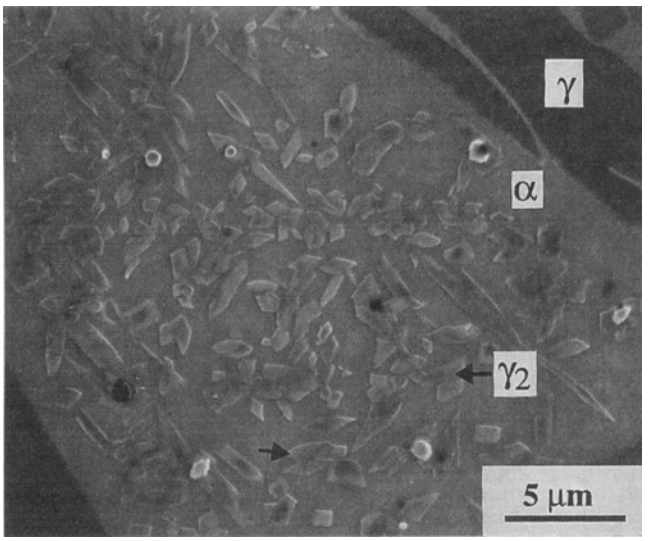

Fig. 2—Ferrite grain in WH-weld metal showing γ_2 with sharp edges. Some γ_2 grains have a midrib in the center (arrowed).

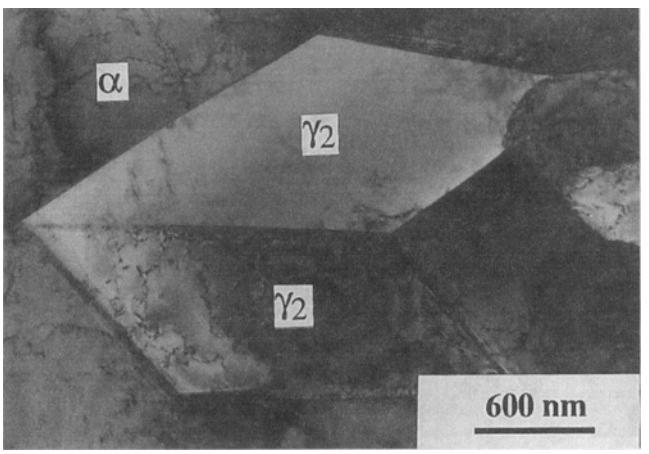

Fig. 3—Micrograph taken in ATEM of a γ_2 grain in WH-weld metal showing a twin boundary in the center.

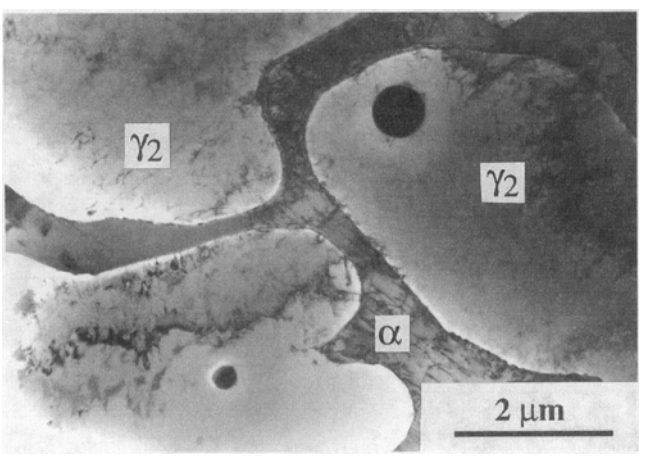

Fig. 4—A γ_2 grain with a globular shape in WH-weld metal (ATEM).

fined crystallographic relation $\langle 0001\rangle_R // \langle 111\rangle_\alpha$ with the ferritic matrix, as shown in Figures 6(a) and (b).

At 800 °C/13.5 min, χ phase and σ phase were identified in all three weld metals, while no R phase was found. The

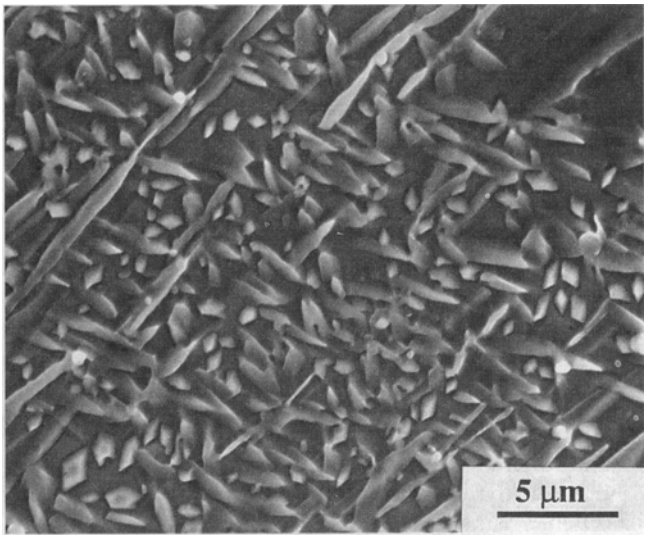

Fig. 5—Secondary austenite in the form of a basket weave structure in WN-weld metal.

Table III. Intermetallic Phases Observed at 700 °C, 800 °C, and 900 °C

Type of Weld Metal	700 °C, 40.5 Min	800 °C, 0.5 Min	800 °C, 13.5 Min	900 °C, 0.5 Min
SD	R,χ	*	σ,χ	σ,χ
WCu	R,χ	*	σ,χ	σ,χ
W	R,χ	mainly χ phase	σ,χ	χ

Not investigated in ATEM.

σ phase seemed to be the most common precipitate in W weld metal after 13.5 minutes of aging, while χ phase was the major precipitate in SD- and WCu- weld metals. However, after only 0.5 minutes of aging at 800 °C, χ phase was predominant also in W-weld metal. An example of σ phase in WCu-weld metal aged at 800 °C/13.5 min is given in Figures 7(a) and (b).

After 0.5 minutes at 900 °C as much as 2.3 pct of intermetallic phase was observed in W-weld metal, while 1.4 and 0.8 pct were found in WCu and SD, respectively. It was interesting to observe that intermetallic phase in W-weld metal was exclusively of the type χ phase an example of which is given in Figures 8(a) and (b). The diffraction pattern in Figure 8(b) illustrates the good matching between the host lattice and that of χ phase and the fact that the orientation relationship was always found to be $\langle 001\rangle_\chi // \langle 001\rangle_\alpha$.

Specimens of all three weld metals containing intermetallic phase were subjected to long-term isothermal heat treatment in steps of 10 °C to assess the dissolution temperature of intermetallic phase. The specimens were subsequently checked by LOM. It was found that the tungsten-rich W-weld metal had a significantly higher dissolution temperature than the other two metals. Experimentally determined values together with temperatures estimated from Thermo-Calc are given in Table IV.

Investigations of all weld metals showed very clearly that χ phase tended to precipitate in narrow ferrite arms while σ phase precipitated essentially in the broad ferrite arms. This tendency could be observed in SEM micrographs us-

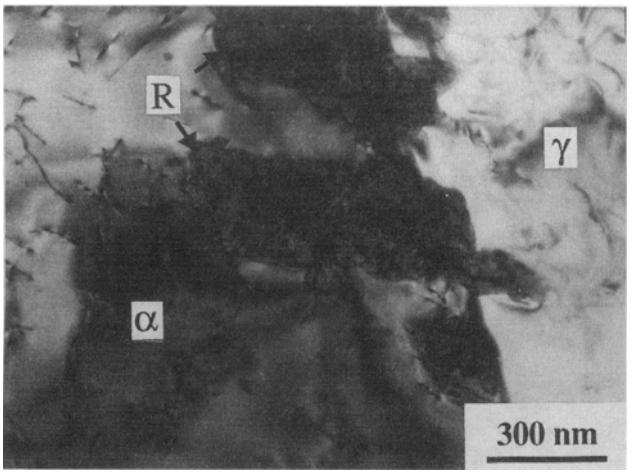

(*a*)

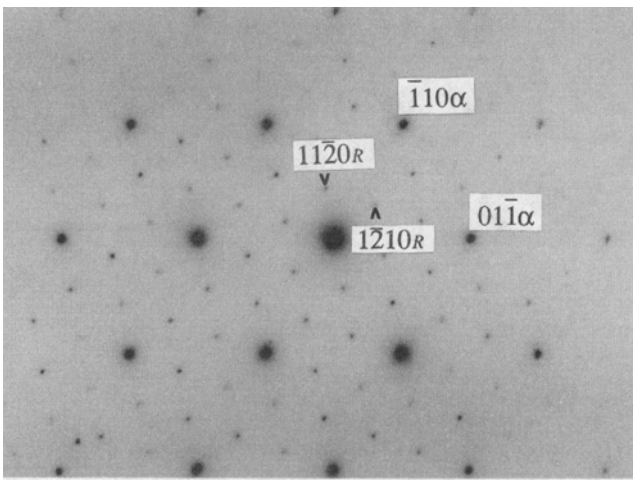

(*b*)

Fig. 6—(*a*) R phase formed in ferrite and at ferrite/austenite boundary in SD-weld metal after aging at 700 °C/40.5 min (ATEM). (*b*) Electron diffraction pattern from zone axis ⟨0001⟩ in *R* phase showing the crystallographic relation $\langle 0001\rangle_R // \langle 111\rangle_\alpha$.

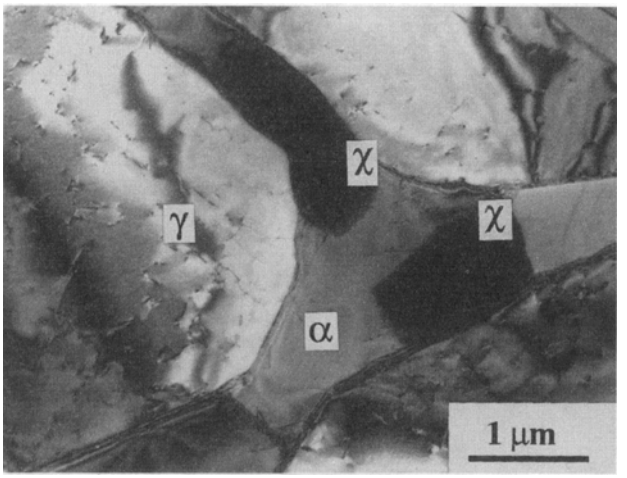

(*a*)

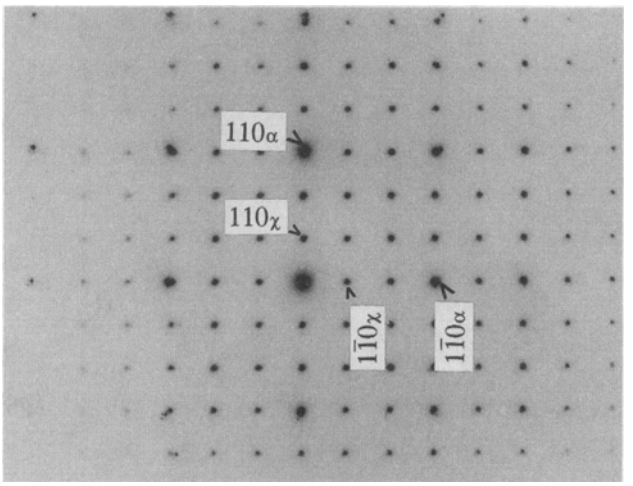

(*b*)

Fig. 7—(*a*) σ phase formed in WCu-weld metal after aging at 800 °C/13.5 min (ATEM). (*b*) Electron diffraction pattern from zone axis ⟨001⟩ in σ phase showing the crystallographic relation $\langle 001\rangle_\sigma // \langle 001\rangle_\alpha$.

ing backscattered electrons, which give rise to atomic number contrast. An example is given in Figure 9 in which the brighter contrast in molybdenum-rich χ phase is evident.

Results from point counting in LOM provided the basis for Avrami curves, TTT diagrams, and CCT diagrams for each weld metal obtained using 0.8 kJ/mm heat input. The time-dependent volume fraction of intermetallic phase determined experimentally (Table V) provided the basis for the Avrami curve. The Avrami curves were found to be suitable to establish the TTT curves since they could be used to extrapolate to shorter times, as in the case of W-weld metal, and to interpolate between discrete experimental values. It is quite clear from the TTT diagram in Figure 10 that 1 pct intermetallic phase is formed much more quickly in W-weld metal. The difference in this respect for WCu- and SD-weld metals is very small, although SD-weld metal appears to be the more stable one. From Figure 11, showing the corresponding 5 pct curve, it can be concluded that WCu- and SD-weld metals are more stable than W-weld metal. This effect is particularly clear at temperatures above 900 °C. The faster kinetics of intermetallic phase formation in W-weld metal is also evident from the values in Table V, in particular from the values obtained at the shortest aging time and at 1000 °C and 1050 °C. From the resulting CCT diagram in Figure 12 calculated according to a procedure described elsewhere,[12] the cooling rates required to avoid 2 pct intermetallic phase can be estimated in terms of cooling curves touching the nose of the CCT curves. The upper part of the CCT curve corresponds to the time necessary to form 1 vol pct of intermetallic phase, while the lower part represents an additional 1 vol pct that will form during cooling to room temperature. The cooling rates corresponding to curves A through E are 720 °C/min, 360 °C/min, 180 °C/min, 90 °C/min, and 45 °C/min, respectively. The critical cooling rate to form 2 pct intermetallic phase was found to be twice as fast for W-weld metal, *viz.* 180 °C/min, compared with 90 °C/min that is required for WCu- and SD-weld metals. To check the validity of the calculated CCT diagram, controlled cooling experiments were performed and the resulting volume fraction of intermetallic phase was measured using point counting. The results for SD-weld metal are presented in Figure 13, in which it is shown that the calculated curve and the experimental values show excellent agreement, provided an adjustment of the time parameters $b(T)$ and $n(T)$ is made.

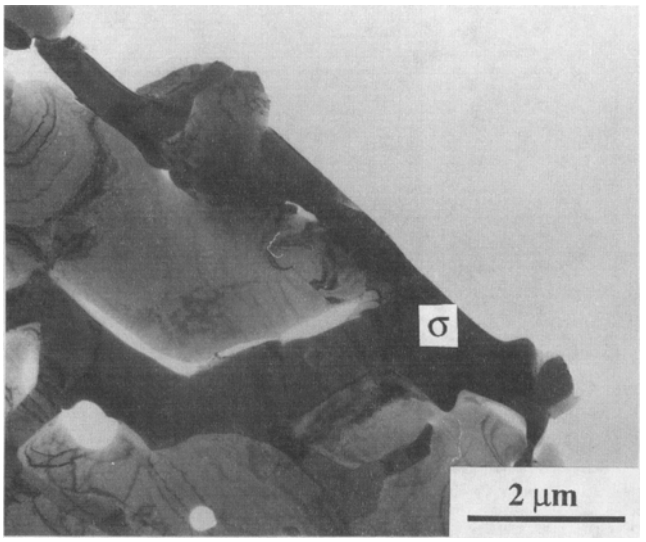

(*a*)

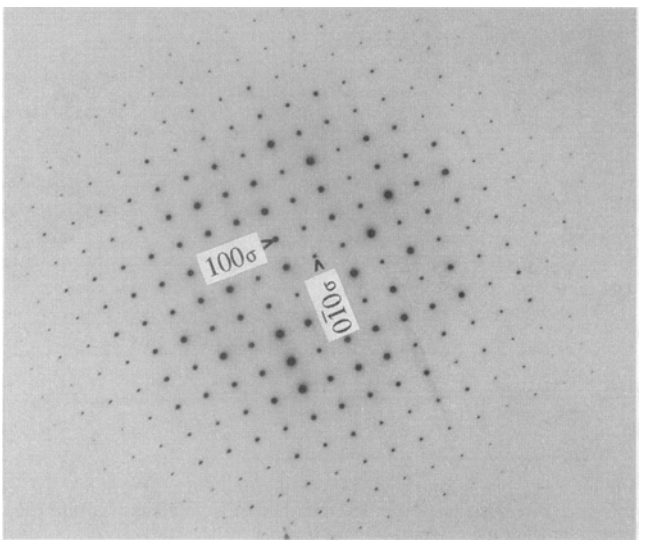

(*b*)

Fig. 8—(*a*) χ phase formed in narrow ferrite regions in WCu-weld metal after aging at 900 °C/0.5 min (ATEM). (*b*) Electron diffraction pattern from zone axis ⟨001⟩ in χ phase showing the crystallographic relation $\langle 001\rangle_\chi // \langle 001\rangle_\alpha$.

B. *Chemical Analyses*

The EDX analyses of precipitates on carbon extraction replicas were performed. It was found that χ phase was rich in molybdenum and tungsten compared with σ phase. Another interesting effect in W-weld metal was the higher concentration of tungsten in χ phase compared with SD- and WCu-weld metal. The measured values are found in Table VI.

The concentration of alloying elements in primary austenite, ferrite, and γ_2 was measured using both EDX and WDX. The EDX analyses in ATEM of the matrix composition showed that the narrow ferrite arms were enriched with molybdenum compared with the broader arms. Quantitative analyses based on the average of 10 measurements showed that the concentration of molybdenum was 5.9 ± 0.3 pct and 5.2 ± 0.4 pct in SD-weld metal, 6.2 ± 0.4 pct and 4.8 ± 0.2 pct in WCu-weld metal, and 5.5 ± 0.4 pct and 4.7 ± 0.4 pct in W-weld metal. In the case of tungsten, there was a tendency toward an enrichment in W-weld metal with measured values of 3.2 ± 0.4 pct in narrow ferrite arms compared with 2.4 ± 0.4 pct in broader ferrite regions. A similar trend regarding tungsten could be observed in WCu-weld metal. However, EDX analysis of WCu-weld metal was not sufficiently accurate to enable a definite conclusion for such low concentrations of tungsten.

A striking observation was also the lower chromium concentration in γ_2 compared with primary austenite. To obtain a higher accuracy and at the same time enable quantification of nitrogen concentration, measurements from WDX in the EPMA were performed. The results from these are presented together with Thermo-Calc predictions in Table VII, in which it can be seen that γ_2 is richer in nickel and poorer in nitrogen compared with primary austenite. To facilitate a comparison between different phases and material conditions, the measured concentrations of the most interesting elements for SD-weld metal at high heat input are illustrated in Figure 14 in the form of a histogram. The results obtained for the other five weld metal conditions are omitted, because they show the same tendency and therefore add no new information. For the sake of consistency, all results in Figure 14 are taken from the WDX analyses in the EPMA. A notable feature is the observed lower concentration of nitrogen and chromium in γ_2. A correspondingly higher concentration of nickel is observed in γ_2. The EDX analysis of γ_2 with a midrib in the center of the type that is imaged in Figure 3 showed that these were particularly poor in chromium; the concentration was found to be 2 to 3 wt pct lower than in the primary austenite.

Table IV. Dissolution Temperatures for Intermetallic Phase (°C)

	SD	WCu	W
Experimental observations	1060	1070	1110
Thermo-Calc	870	920	970

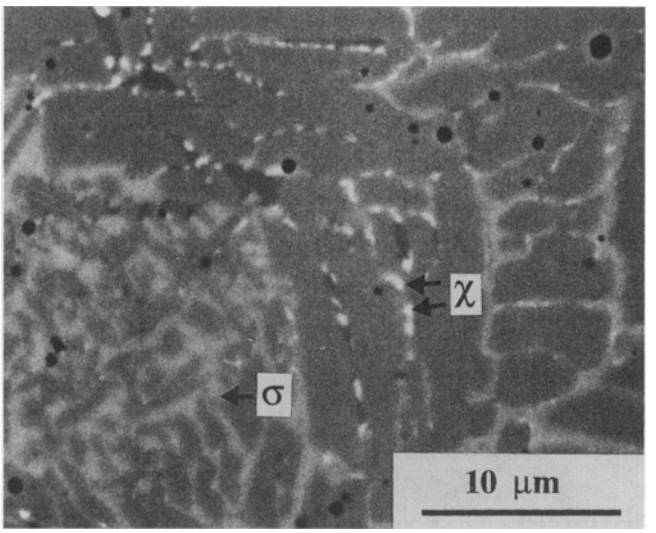

Fig. 9—Backscattered electron micrograph from WCu-weld metal aged at 800 °C/13.5 min showing χ phase in brightest contrast in narrow ferrite arms and σ phase in gray contrast in broader ferrite regions (SEM).

Table V. Volume Fraction of Intermetallic Phase in Normal Heat Input (0.8 kJ/mm) Weld Metal Determined by Point Counting

	0.5 Min	1.5 Min	4.5 Min	13.5 Min	40.5 Min	121.5 Min
1050 °C, SD	0.1 ± 0.1	0.2 ± 0.2	0.1 ± 0.1	1.1 ± 0.8	1.4 ± 0.7	4.5 ± 1.5
1050 °C, WCu	0.1 ± 0.1	0.4 ± 0.4	0.4 ± 0.4	1.5 ± 1.2	2.3 ± 1.0	6.2 ± 1.8
1050 °C, W	1.7 ± 0.7	2.4 ± 1.0	7.0 ± 1.5	11.4 ± 1.9	15.8 ± 2.4	24.8 ± 2.2
1000 °C, SD	0.6 ± 0.4	3.3 ± 1.4	4.8 ± 1.3	13.0 ± 2.5	18.9 ± 2.6	22.0 ± 2.8
1000 °C, WCu	0.7 ± 0.5	2.5 ± 1.1	6.6 ± 2.0	16.5 ± 2.4	21.1 ± 2.4	22.5 ± 2.5
1000 °C, W	3.1 ± 1.0	8.3 ± 1.5	19.2 ± 2.1	26.1 ± 2.2	33.9 ± 2.3	34.4 ± 2.3
950 °C, SD	0.4 ± 0.4	2.8 ± 1.3	11.3 ± 2.7	19.1 ± 3.1	—	—
950 °C, WCu	1.5 ± 0.7	3.4 ± 1.2	12.5 ± 2.0	18.9 ± 2.3	—	—
950 °C, W	1.7 ± 0.7	4.6 ± 1.2	10.9 ± 1.8	12.2 ± 1.7	—	—
900 °C, SD	0.8 ± 0.5	3.5 ± 1.7	11.2 ± 2.7	17.2 ± 2.3	—	—
900 °C, WCu	1.4 ± 0.6	3.0 ± 1.1	10.5 ± 2.2	17.1 ± 2.0	—	—
900 °C, W	2.3 ± 1.2	3.4 ± 1.0	5.0 ± 1.1	11.9 ± 1.6	—	—
850 °C, SD	0.7 ± 0.5	2.2 ± 1.0	6.4 ± 1.8	16.8 ± 2.3	—	—
850 °C, WCu	0.9 ± 0.6	1.8 ± 0.9	8.0 ± 1.4	16.5 ± 1.2	—	—
850 °C, W	2.6 ± 0.8	3.7 ± 1.1	5.2 ± 1.0	7.9 ± 1.3	—	—
800 °C, SD	0.9 ± 0.6	1.2 ± 0.6	2.0 ± 0.8	5.6 ± 1.5	12.3 ± 1.7	—
800 °C, WCu	0.7 ± 0.5	1.0 ± 0.6	3.0 ± 1.3	10.8 ± 1.7	16.5 ± 2.3	—
800 °C, W	2.0 ± 0.8	3.6 ± 1.2	4.8 ± 1.1	7.0 ± 1.1	10.1 ± 1.3	—
750 °C, SD	—	—	0.7 ± 0.5	1.9 ± 0.9	3.9 ± 1.1	11.9 ± 1.9
750 °C, WCu	—	—	1.6 ± 0.7	2.5 ± 1.0	7.9 ± 1.6	15.4 ± 2.2
750 °C, W	—	—	3.5 ± 1.0	4.2 ± 1.1	7.7 ± 1.4	14.1 ± 2.2
700 °C, SD	—	—	—	0.4 ± 0.4	1.6 ± 0.8	4.7 ± 1.3
700 °C, WCu	—	—	—	1.5 ± 0.9	2.7 ± 0.9	4.8 ± 1.1
700 °C, W	—	—	—	3.4 ± 1.1	3.8 ± 1.0	5.3 ± 1.2

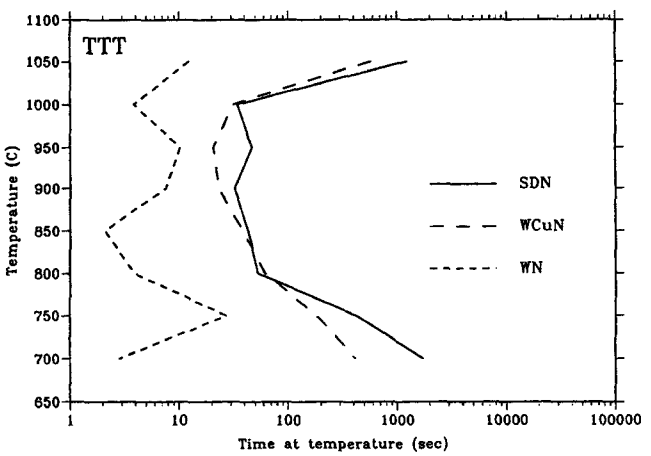

Fig. 10—TTT diagram of all three weld metals showing C curves representing 1 pct of intermetallic phase. C curve of W-weld metal is displaced toward shorter times than those of WCu and SD-weld metals.

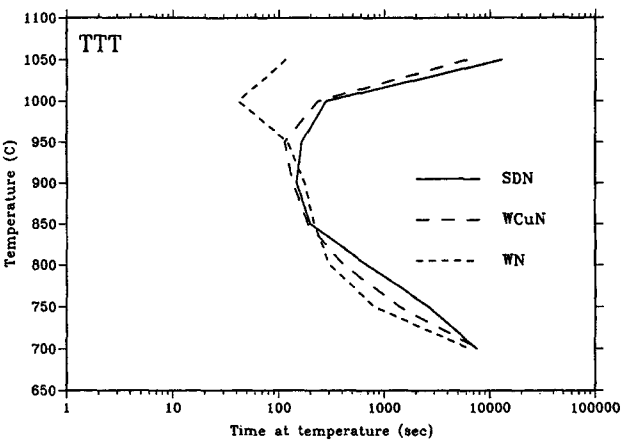

Fig. 11—TTT diagram of all three weld metals showing C curves representing 5 pct of intermetallic phase. C curve of W-weld metal is displaced toward shorter times above about 900 °C.

C. *Equilibrium Calculations by Thermo-Calc*

The temperature dependence of phases obtained by Thermo-Calc is shown in Figure 15, from which it can be seen that the fraction of ferrite decreases and austenite increases rapidly with decreasing temperature below 1300 °C. The diagram was calculated based on the chemical composition of W-weld metal, but the principal appearance is the same for SD- and WCu-weld metal. It can also be seen in Figure 15 that the onset of σ phase and Cr_2N occurs in the temperature interval 900 °C to 1000 °C. However, these precipitates were excluded in modeling the formation of γ_2, since they were rarely observed in the nonequilibrium as-welded condition. The formation of secondary austenite during reheating can be understood from the fact that there is a corresponding increase in equilibrium fraction of austenite, as can be seen in Figure 15. If it is assumed that primary austenite and ferrite are formed at 1300 °C and secondary austenite is formed at 800 °C under the conditions described in Section II, the concentrations of elements can be estimated from Thermo-Calc. The results obtained for SDN-, WCuN-, and WN-weld metals are collected in Table VII, in which WDX results are shown in parentheses. It is assumed that the composition of primary austenite (γ) is determined at 1300 °C and that of γ_2 at 800 °C. It is shown in Table VII that Thermo-Calc is capable of predicting the experimentally observed lower concentrations of chromium and nitrogen in γ_2 compared with primary austenite. In the case of chromium, there is a discrepancy in absolute values, but the correct tendency is predicted. In the case of nitrogen, the observed values all fall in between the values corresponding to the upper and lower bounds.

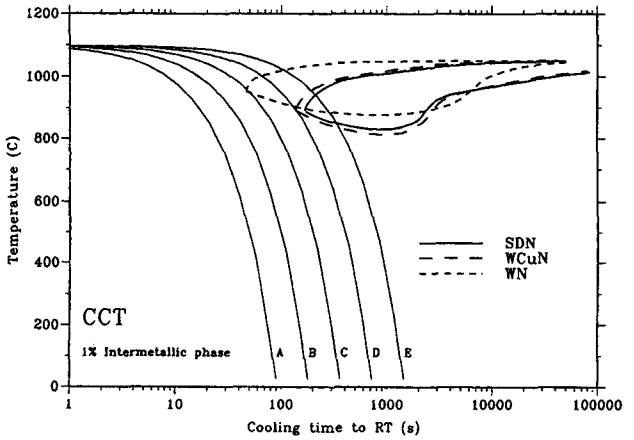

Fig. 12—CCT curves for cooling rates in the range 720 °C/min to 45 °C/min. Cooling curve touching the nose of a CCT curve indicates that 2 vol pct of intermetallic phase will form during cooling. This critical cooling rate was found to be 180 °C/min for W- and 90 °C/min for WCu- and SD-weld metals.

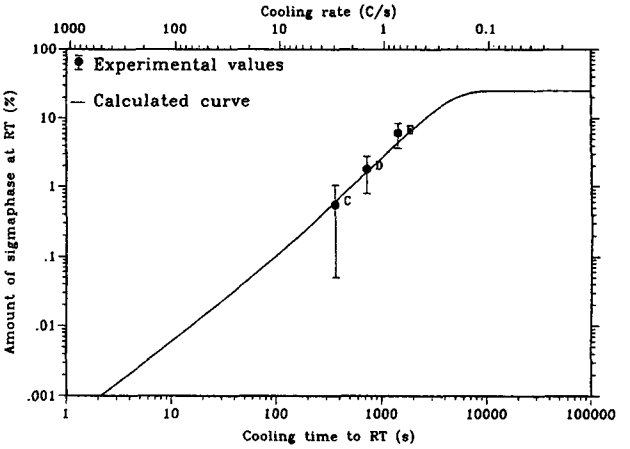

Fig. 13—Volume percentage of intermetallic phase as a function of cooling rate in SDN. Comparison between calculated and experimentally obtained values.

IV. DISCUSSION

A. *Intermetallic Phase*

It is clear from the TTT diagrams in Figures 10 and 11 and in the CCT diagram in Figure 12 that tungsten-rich weld metal is more prone to intermetallic phase formation. Not only is the observed volume percentage of intermetallic phase higher after long-term aging in tungsten-rich weld metal, ~35 pct at 1000 °C compared with ~25 pct at 1000 °C in WCu- and SD-weld metal, but it is also evident from the results of point counting in Table V that the kinetics is much faster. In addition, the temperature range of stability in tungsten-rich weld metal is extended to 1110 °C compared with 1070 °C for WCu- and 1060 °C for SD-weld metals. A closer examination of the values obtained at 0.5 minutes in Table V shows that the formation of intermetallic phase is significantly faster in tungsten-rich weld metal in the entire temperature range from 700 °C to 1050 °C, but the effect is most pronounced in the upper part of this range. These results are consistent with the observations of Charles,[3] are intimately related to the presence of tungsten, and can be rationalized as follows.

The EDX analyses of the chemical composition of the intermetallic phases, σ phase and χ phase, show a strong affinity to tungsten in addition to chromium and molybdenum. This is interpreted as evidence that tungsten stabilizes both σ phase and χ phase. This is also consistent with the equilibrium concentrations predicted from Thermo-Calc, as presented in Table VI. Although in the case of tungsten these are higher than the observed nonequilibrium values, they clearly confirm this trend. As a consequence, the driving force for intermetallic phase formation will tend to increase with additions of tungsten.

An additional effect, which is quite essential to explain the faster kinetics in tungsten-rich weld metal, is the ease with which intermetallic phase nucleates. Because of the tetragonal structure of σ phase, there is a large mismatch with the ferritic matrix.[16] Nucleation of σ phase, therefore, is associated with large coherency strains and, therefore, is comparatively difficult. However, nucleation of χ phase is relatively easy because of its cubic structure and a lattice parameter that is very close to 3 times that of ferrite.[17] As observed in this investigation as well as in a previous investigations of superduplex stainless steel base metal,[5] only σ phase is present after very long aging times while χ phase appears after very short aging times and subsequently dissolves. A similar precipitation sequence was observed by Vitek and David[18] in a duplex-type 308CRE alloy in which G phase precipitated first and later dissolved while σ phase was the only precipitate present after longer aging times. Moreover, according to Thermo-Calc, χ phase is not thermodynamically stable for the compositional ranges and temperature ranges discussed here. These observations support the view that χ phase precipitates as a metastable phase prior to σ phase because of easier nucleation. Since analyses using Thermo-Calc and EDX both showed an enrichment of tungsten in χ phase, it is suggested that the faster kinetics of intermetallic precipitation in tungsten-rich weld metal is due to a higher driving force for the precipitation of χ phase caused by the very presence of tungsten.

It has been suggested that intermetallic phase formation is suppressed in duplex stainless steel base metal in which molybdenum is replaced by tungsten owing to slower diffusion of tungsten.[2,19] The present investigation, based on the behavior of weld metal, has clearly shown that there is an adverse effect of tungsten. The faster kinetics of intermetallic phase formation seems to be attributable to easier nucleation rather than enhanced diffusivities. Results from Fridberg *et al.*[20] lend support to this view *via* a review article in which it is shown that the diffusivities of tungsten and molybdenum in ferrite are virtually equal. These authors found a diffusion coefficient of 1.0 cm^2/s and an activation energy of 240 kJ/mole for both tungsten and molybdenum. Although a weld metal is structurally more unstable owing to ample quenched-in nuclei in combination with chemical concentration gradients,[7] the tendency can be expected to be qualitatively the same in the base metal.

Observation of preferential formation of χ phase in narrow ferrite arms in combination with an enrichment of molybdenum in these is an interesting phenomenon, because it illustrates very clearly how the formation of χ phase is promoted by the presence of molybdenum. The enrichment of molybdenum is a result of the rejection of ferrite stabilizing molybdenum from the abutting austenite. Although

Table VI. Chemical Composition* of Precipitates after Aging 13.5 Minutes at 850 °C Obtained by EDX Analysis in ATEM and Calculated by Thermo-Calc (in Parentheses)

Phase	Weld Metal	Fe	Mn	Cr	Ni	Mo	W
σ phase	SD	bal	0.7(0.0)	29.7(40.8)	5.0(6.2)	6.2(12.4)	—
σ phase	WCu	bal	1.4(0.0)	28.5(40.0)	5.6(4.4)	5.4 (8.6)	1.6 (2.3)
σ phase	W	bal	1.3(0.0)	30.0(39.5)	4.5(5.4)	6.8 (8.4)	4.4 (8.1)
χ phase	SD	bal	0.8(0.0)	27.4(27.8)	5.4(0.0)	11.9(21.4)	—
χ phase	WCu	bal	0.7(0.0)	26.8(26.6)	4.1(0.0)	12.0(16.6)	3.4 (7.0)
χ phase	W	bal	1.1(0.0)	26.6(25.9)	2.9(0.0)	17.0(11.3)	12.7(19.0)

*Experimental uncertainties are typical of the EDX technique, *i.e.*, between 0.3 (Ni) and 0.7 (Fe) wt pct for all elements.

Table VII. Concentration in Weight Percent of Alloying Elements in Austenite and Ferrite Measured by WDX (in Parentheses) and Estimated by Thermo-Calc at 1300 °C and 800 °C (Composition Equal to Chemical Composition Obtained by OES, Table I)

		Cr	Mo	N	Ni	Cu	W
γ, 1300 °C	SD	23.8(25.5)*	2.9(3.3)	0.50(0.43)	11.5 (9.6)	—	—
γ, 1300 °C	WCu	23.3(25.1)	2.7(3.1)	0.42(0.54)	11.5 (9.7)	0.91(0.68)	0.75(0.54)
γ, 1300 °C	W	23.6(25.9)	2.3(2.4)	0.48(0.48)	12.2(10.5)	—	1.9 (1.6)
α, 1300 °C	SD	26.6(26.0)	4.3(3.9)	0.09(0.04)	7.9 (8.5)	—	—
α, 1300 °C	WCu	27.0(26.5)	4.2(4.0)	0.09(0.08)	7.6 (7.8)	0.41(0.63)	1.04(0.60)
α, 1300 °C	W	26.9(26.9)	3.6(2.8)	0.10(0.13)	8.1 (9.0)	—	2.6 (1.7)
γ_2, case 1	SD	23.6	3.3	0.32	10.7	—	—
γ_2, case 1	WCu	23.1	3.1	0.30	10.8	0.76	0.75
γ_2, case 1	W	23.3	2.6	0.32	11.5	—	1.9
γ_2, case 2	SD	21.7	3.5	0.16	12.5	—	—
γ_2, case 2	WCu	21.4	3.2	0.18	11.3	0.71	0.69
γ_2, case 2	W	21.6	2.7	0.19	12.0	—	1.7
γ_2, WDX*	SD	(24.9)	(2.9)	(0.21)	(11.1)	—	—
γ_2, WDX	WCu	(24.1)	(2.6)	(0.22)	(10.69)	(0.79)	(0.42)
γ_2, WDX	W	(25.1)	(2.4)	(0.26)	(11.0)	—	(1.2)

*Values in parentheses were obtained by WDX analyses in the EPMA.

a similar effect can be expected for tungsten, it was not sufficiently pronounced to be detected by EDX analysis.

B. *Secondary Austenite*

Previous investigations of γ_2 using Thermo-Calc have predicted lower concentrations of nitrogen and chromium compared with primary austenite.[5,6] The conclusion has been shown to be qualitatively valid for γ_2 being formed in a wide temperature range below 1300 °C assuming that primary austenite forms at 1300 °C.[6] In the case of chromium, this has been verified quantitatively using EDX analyses.[5,6,21,22] However, in the case of nitrogen, there is only qualitative information available in the literature from secondary ion mass spectrometry in support of the thermodynamic calculations.[6] An important aspect of the present investigation is that it demonstrates that low energy WDX analysis in EPMA offers a viable technique for measuring quantitatively also the concentration of nitrogen in γ_2 provided the diameter of the γ_2 grains exceeds 1 to 2 μm, which corresponds to the spatial resolution of this technique. The observed concentrations of nitrogen, *viz.* 0.21 to 0.26 wt pct, are in good agreement with the predictions from Thermo-Calc, which predicts nitrogen concentrations in the range 0.16 to 0.32 wt pct depending upon the approach used to model the formation of γ_2.

It is important to emphasize that thermodynamic equilibrium will never be attained in a weld metal because of the rapid cooling. The weld metal, therefore, is to be regarded as a highly metastable structure. Nevertheless, the present investigation has shown that it is possible to model the essential features of the weld metal in DSS by the computer program Thermo-Calc. This has been accomplished by considering two extreme cases, an upper and a lower bound, between which the real case is assumed to lie. The upper bound corresponds to the unlikely event of equilibrium between γ_2, primary austenite, and ferrite (case 1), while the lower bound considers the case when the composition in primary austenite is frozen at 1300 °C and only equilibration between γ_2 and the ferrite occurs (case 2). It should be mentioned that intermetallic phase (σ phase) and Cr_2N, which are expected in thermal equilibrium, are omitted in the calculations. This can be justified because these phases were virtually absent in as-welded material in the present investigation. The absence of intermetallic phase and Cr_2N is taken as evidence that the thermal cycles during welding were too short for the precipitation of intermetallic phase but involved sufficiently slow cooling rates for nitrogen to be accommodated in solid solution in the austenite. In case, 1, a high concentration of nitrogen can be expected in γ_2, since there are no restrictions regarding diffusion of alloying elements between ferrite and primary austenite. A low concentration of nitrogen can be expected in case 2, since nitrogen in the primary austenite is inaccessible to the γ_2. However, in practice, it is estimated that some exchange of alloying elements between primary austenite and ferrite occurs. This is particularly the case for rapidly diffusing interstitials. The experimental observation of nitrogen

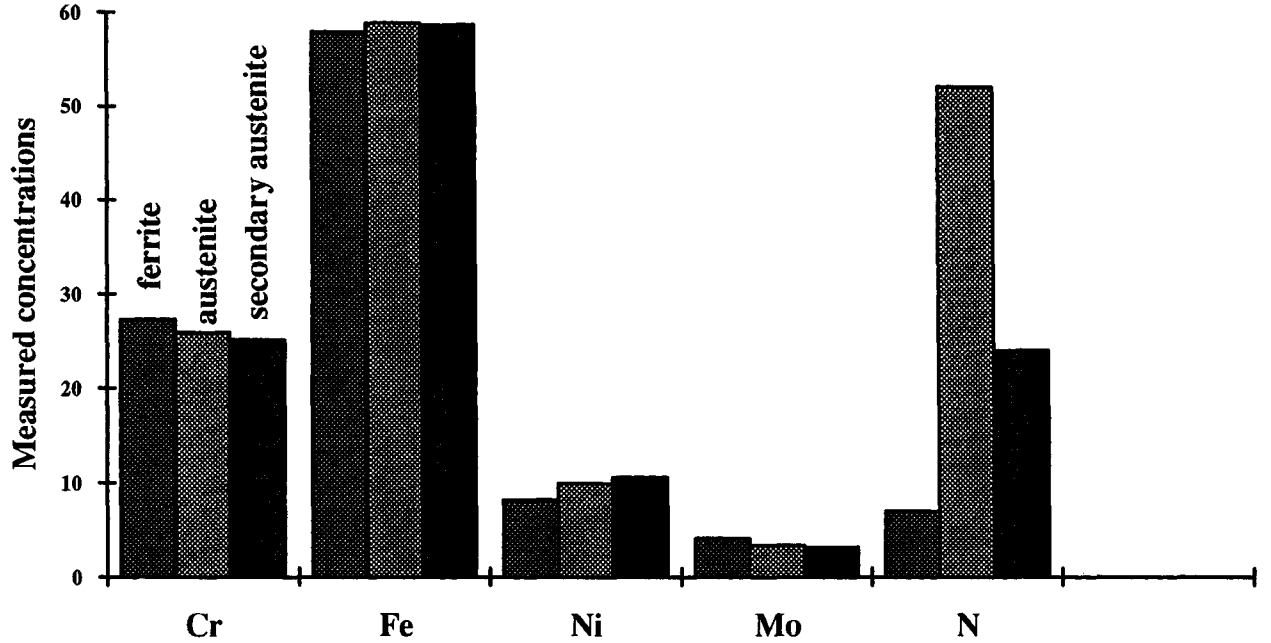

Fig. 14—Measured concentrations of Cr, Fe, Ni, and Mo in wt pct and for N in wt pct × 100 obtained in SDH-weld metal using WDX in EPMA.

concentrations well within the predicted interval 0.16 to 0.32 wt pct confirms that the modeling of γ_2 formation used in the present investigation is quite realistic.

In the case of chromium, Thermo-Calc predicts a concentration in γ_2 that is lower than that in primary austenite. This tendency is also observed experimentally using WDX, although it must be pointed out that the absolute experimental values are unrealistically high bearing in mind that the average concentration of chromium should be 25 pct. The discrepancy is most likely caused by a systematic error associated with the WDX technique. A comparison with the results from optical emission spectroscopy suggests that the error is typically 2.0 wt pct. If this error is taken into account, good agreement between WDX analyses and Thermo-Calc is obtained. This also shows that the assumption that γ_2 is formed at about 800 °C is quite realistic.

The observation of different tendencies to form γ_2 in different weld metals produced under identical welding conditions is interesting, since it shows that its formation is highly dependent on chemical composition. A stronger tendency to form γ_2 in WCu- and W-weld metals is quite evident from the microstructural investigations (Table II and Figures 1(a) through (c)). This effect can be given a physical interpretation following the argument of Hertzman *et al.*[11] The driving force for precipitation of γ_2 is assumed to be proportional to $f_{eq} - f_{\text{rapid}}$, where f_{eq} is the volume fraction of γ_2 in true thermodynamic equilibrium at 1000 °C and f_{rapid} is the volume fraction of γ_2 calculated assuming paraequilibrium conditions during cooling. Their calculations show that under these assumptions, W- and WCu-weld metal show a stronger tendency to form γ_2. Although this interpretation provides a very likely physical explanation, the role of tungsten and copper in the nucleation of γ_2 cannot be entirely ignored. However, an estimation of this requires analytical techniques at atomic resolution and was beyond the scope of this investigation.

The morphology of γ_2 deserves some comments. Essentially, two types of morphologies of γ_2 were observed, a Widmannstätten type with sharp edges (Figure 3) and a globular type (Figure 4). The Widmannstätten type includes γ_2 grains with a midrib. Such γ_2 grains have also been observed by Solomon and Devine[23] and identified by Nilsson *et al.*[6] to be two austenite crystals separated by a twin boundary. It is interesting to note that γ_2 with a midrib showed even lower concentrations of chromium than other types of γ_2. However, the reason for this is not clear to the authors.

C. *Effect on Properties*

Results obtained by Hertzman *et al.*[11] on identical weld metals show toughness and corrosion properties that are explicable on the basis of the previously mentioned microstructural findings. These authors found a rapid embrittlement of W-weld metal with aging time when testing impact toughness at room temperature. Already after 10 seconds of aging in the temperature range 850 °C to 950 °C, critical toughness values close to the accepted limit 27 J were obtained. This is intimately related to the early formation of intermetallic phase in tungsten-rich weld metal. Corrosion properties as a function of previous aging time at 900 °C were also determined using electrochemical testing in a solution of 1 M NaCl. WCu-weld metal exhibited significantly lower critical pitting temperatures than W- and SD-weld metals, the difference being at least 5 °C. This effect in part can be attributed to the large volume fraction of γ_2 in WCu-weld metal. A slightly lower corrosion resistance was observed also in W-weld metal, particularly for aging times beyond 30 seconds, indicating that there was an effect of intermetallic phase also on the corrosion behavior. However, the fact that W-weld metal is comparable with SD-weld metal in unaged condition despite significant amounts of γ_2 most likely reflects the observed beneficial effect of tungsten in solid solution on pitting resistance.[19]

A final comment relates to the experience from welding

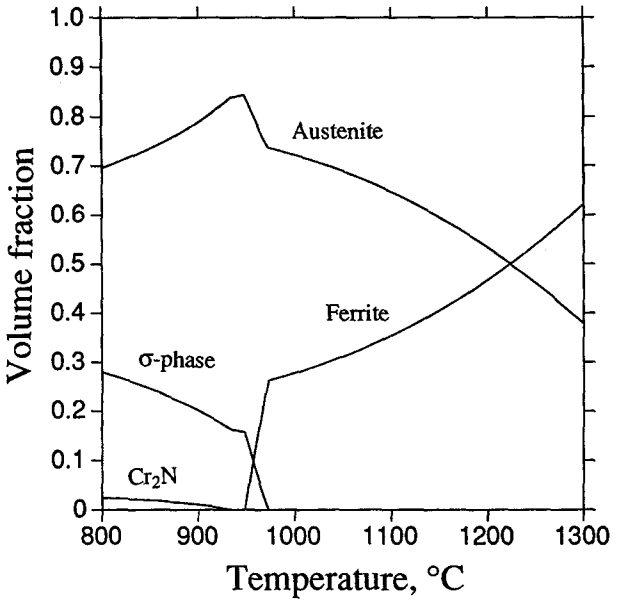

Fig. 15—Diagram obtained by Thermo-Calc based on the composition of W-weld metal showing the dependence of equilibrium volume fraction on temperature of the phases austenite, ferrite, σ phase, and Cr_2N.

practice of SDSS. Although it is not possible to guarantee a weld that is entirely free of γ_2, it is important to emphasize that no practical problems have been encountered in SD-weld metal. This can be understood from the fact that γ_2 is not exposed to the surface and only confined to the interior of reheated weld beads in combination with its low volume fraction. However, the present investigation has shown that the tendency to form γ_2 is a very sensitive function of chemical composition. This is also the case with intermetallic phases in duplex stainless steel weld metal. In W- and WCu-weld metal, the tendency to form γ_2 was found to be sufficiently strong to result in γ_2 also in surface regions, which implies that γ_2 will be exposed to the environment. This is expected to have an adverse effect on the corrosion properties.[5,6] The term γ_2 is also a sensitive function of the welding parameters. During welding of pipes, the formation of γ_2 in duplex stainless steel weld metal can be suppressed by using a relatively low heat input in the second pass. By using this technique, experience has shown that no γ_2 will be formed in SD-weld metal in the surface region of the root bead. In practice, intermetallic phase formation can also be avoided in SD-weld metal provided the welding recommendations are followed. However, it can be inferred from the present investigation (Figure 12) that this is more difficult to achieve in tungsten-rich weld metal because of the faster cooling rate required to avoid precipitation of intermetallic phase.

V. CONCLUSIONS

1. Tungsten-rich weld metal showed faster kinetics of intermetallic phase formation and a higher dissolution temperature of intermetallic phase compared with tungsten-poor and tungsten-free weld metals. This susceptibility to intermetallic precipitation was found to be due to tungsten, which presumably decreases the free energy of formation of nonequilibrium χ phase.
2. Microstructural observations show that the nucleation of χ phase is associated with small coherency strains. This offers a likely explanation for the earlier precipitation of χ phase compared with σ phase.
3. Intragranular secondary austenite in all weld metals investigated was found to be depleted in chromium and nitrogen relative to primary austenite. The concentration of nitrogen was measured by WDX analysis to be in the range 0.21 to 0.26 wt pct in γ_2 compared with 0.48 to 0.54 wt pct in primary austenite.
4. The formation of γ_2 was modeled using Thermo-Calc. The prediction of concentrations of elements in austenite, ferrite, and secondary austenite was in good agreement with experimentally measured values using EDX and WDX.
5. Tungsten bearing and tungsten + copper bearing weld metals were found to be more susceptible to formation of γ_2 than weld metal devoid of these elements. This resulted in γ_2 in the surface regions in tungsten and tungsten + copper weld metals, while no such effect was observed in weld metal in the absence of tungsten and copper.

ACKNOWLEDGMENTS

This article is published by permission of AB Sandvik Steel, Esab AB, and the Swedish Institute for Metals Research. The encouragement from Drs. B. Berglund and S Hertzman and the technical assistance of Messrs. R. Ekrud, Å. Karlsson, and J. Lindqvist are gratefully acknowledged. Support from A. Brorson, Avesta-Sheffield AB, and P. Nerman, Avesta-Sandvik Tube, is appreciated.

REFERENCES

1. J.-O. Nilsson: *Mater. Sci. Technol.*, 1992, vol. 8, pp. 685-700.
2. H. Okamoto, K. Tsuda, S. Azuma, M. Ueda, and K. Ogawa: Paper to appear in *Duplex Stainless Steels '94*, Proc. Conf., Glasgow, England, Nov. 14–16, 1994, The Welding Institute, Cambridge, United Kingdom, 1995, paper 91.
3. J. Charles: *Duplex Stainless Steels '91*, Proc. Conf., Les Editions de Physique, Paris, 1991, vol. 1, pp. 3-48.
4. H.D. Solomon and T.M. Devine: *Duplex Stainless Steels*, Proc. Conf., R.A. Lula, ed., ASM, Metals Park, OH, 1984, pp. 693-756.
5. J.-O. Nilsson and A. Wilson: *Mater. Sci. Technol.*, 1993, vol. 9, pp. 545-54.
6. J.-O. Nilsson, L. Karlsson, and J.-O. Andersson: *Mater. Sci. Technol.*, 1995, vol. 11, pp. 276-83.
7. K. Easterling: *Introduction to the Physical Metallurgy of Welding*, 1st ed., Butterworth & Co. Ltd., London, 1983, pp. 48-103.
8. A.J. Sedriks: *Corrosion*, 1989, vol. 45, pp. 510-18.
9. L. Karlsson and S. Pak: *12th Int. Corrosion Congr.*, Proc. Conf., Houston, TX, Sept. 19–25, 1993, NACE, Houston, TX, 1993, vol. 4, pp. 2944-58.
10. B. Lundqvist, K. Olsson, and P. Norberg: *Duplex Stainless Steel '86*, Proc. Conf., Nederlands Instituut voor Lastechniek, The Hague, 1986, pp. 16-29.
11. S. Hertzman, M. Nilsson, and R. Jargelius-Pettersson: *Proc. 4th Int. Conf. Duplex Stainless Steels*, Glasgow, Scotland, Nov. 13–16, 1994, The Welding Institute, Abington Publishing, Cambridge, England, 1995, vol. 1, paper 1.
12. B. Josefsson, J.-O. Nilsson, and A. Wilson: *Duplex Stainless Steels '91*, Proc. Conf., Les Editions de Physique, Paris, 1991, vol. 1, pp. 67-78.
13. E. Beraha and B. Shpigler: *Color Metallography*, 1st ed., ASM, Metals Park, OH, 1977.
14. O. Hedebrant: *Jernkontorets Ann.*, 1954, vol. 138 (10), pp. 643-54.
15. B. Sundman, B. Jansson, and J.-O. Andersson: *CALPHAD*, 1985, vol. 9, pp. 153-90.
16. E.O. Hall and S.H. Algie: *Metall. Rev.*, 1966, vol. 11, pp. 61-88.
17. J.S. Kasper: *Acta Metall.*, 1954, vol. 2, pp. 456-61.

18. J.M. Vitek and S.A. David: *Metall. Trans. A*, 1987, vol. 18A, pp. 1195-1201.
19. H. Okamoto: *Applications of Stainless Steels '92*, Proc. Conf., The Institute of Materials, Stockholm, 1992, vol. 1, pp. 360-69.
20. J. Fridberg, L.-E. Törndahl, and M. Hillert: *Jernkont. Ann.*, 1969, vol. 153, pp. 263-76.
21. C.V. Roscoe, K.J. Gradwell, and G.W. Lorimer: *Stainless Steels '84*, Proc. Conf., Göteborg, Sweden, The Institute of Metals, London, 1984, pp. 563-77.
22. L. Karlsson and S. Pak: *Stainless Steels '91*, Proc. Conf., Chiba, Japan, The Iron and Steel Institute of Japan, 1-9-4 Otemachi Chiyoda-ku Tokyo 100, Japan, 1991, vol. 2, pp. 1101-08.
23. H.D. Solomon and T.M. Devine: ASTM STP 672, ASTM, Philadelphia, 1979, pp. 430-61.